metals

Article

Enhancement of Fatigue Endurance by Al-Si Coating in Hot-Stamping Boron Steel Sheet

Yuqiang Li [1], Ning Tan [2], Zhishuai Xu [1], Zhiping Luo [3], Ke Han [4], Qijie Zhai [1] and Hongxing Zheng [1,*]

1 Center for Advanced Solidification Technology, School of Materials Science and Engineering, Shanghai University, Shanghai 200444, China
2 Baosteel Central Research Institute, Shanghai 201900, China
3 Department of Chemistry and Physics, Fayetteville State University, Fayetteville, NC 28301, USA
4 National High Magnetic Field Laboratory, Florida State University, Tallahassee, FL 32310, USA
* Correspondence: hxzheng@shu.edu.cn; Tel.: +86-137-6135-6748

Received: 2 June 2019; Accepted: 24 June 2019; Published: 26 June 2019

Abstract: Most structural components undertake cyclic loads in engineering and failures always cause catastrophic economic losses and casualties. In the present work, the phase evolution of Al-Si coating of high-strength boron steel during hot stamping was investigated. Two types of 1500 MPa grade boron steel sheets, one with Al-Si coating and the other without, were studied to reveal the effect on the high-cycle fatigue behavior. The as-received continuously hot-dip Al-Si coating was composed of α(Al), eutectic Al-Si and τ_5. After hot stamping at 1193 K, three phases formed in this coating: β_2, Fe(Al,Si)$_2$ and α(Fe). The experimental results showed that the endurance limit of the coated steel sheet was 370 MPa under 10^7 fully reversed tension-compression loading cycles as opposed to 305 MPa in the uncoated sheet. Both the coated and the uncoated specimens showed surface-induced transgranular fatigue fractures. In the uncoated sheet, the fatigue cracks were generated from the decarburization surface, but the Al-Si coating effectively prevented the occurrence of near-surface decarburization during high-temperature hot stamping, and the only cracks in the coated steel sheet were initiated at wire-cutting surfaces.

Keywords: boron steel; Al-Si coating; hot stamping; high-cycle fatigue; decarburization

1. Introduction

Demands for increasing safety, reducing the weight of automobile bodies and fuel consumption in automotive manufacturing have promoted technological innovation [1–4]. Due to high stamping loads, large spring-backs, bad formability and severe wear such as galling and seizure, cold stamping of high strength steels is facing challenges [5,6]. Hot stamping has been rapidly developed since it effectively overcomes/avoids these problems, and presently it can be roughly classified into direct and indirect methods according to technological routes [7]. For the direct hot stamping process, the steel sheet is heated firstly, transferred to the press and subsequently formed and quenched in a closed tool [8]. In contrast, a pre-formed part is cold-stamped firstly in case of the indirect hot stamping process, and only quenching and calibration are performed after austenitizing in the press [9]. On the other hand, boron steel sheets have been widely used for the production of high strength panels of car bodies and vehicle chassis structures due to its excellent formability [10,11]. The ultimate tensile strength of hot-stamping boron steel sheets would reach up to 1500 MPa with a full martensite microstructure [12,13]. Nevertheless, it was inevitable that bare (uncoated) steel sheets were thermally oxidized in earlier hot stamping technology and the oxidized scale had to be removed by shot blasting or shot peening [14]. Subsequently, the attempt to use lubricant oils was abandoned due to complex cleaning procedures and a high risk for hydrogen-induced embrittlement [15]. Currently, various types of coatings, including aluminized coating [16–20], galvanized and galvannealed coatings [21–23], Zn-Ni alloy coating [24,25], sol-gel hybrid coating [26] and Al-Zn alloy coating [27], were developed industrially. Among which, Type 1 aluminized coating, Al-Si with a near eutectic composition, has been widely applied on high-strength boron steel sheets [28].

Currently, the relationship between mechanical properties (e.g., toughness and hardness etc.), microstructure (e.g., phase constitution and morphology, etc.) and hot-stamping parameters (e.g., autenitization temperature and holding duration, etc.) of boron steel sheets have been extensively reported [29–31]. However, most structural components of automobiles are indeed exposed to cyclic loads or continuous vibrations during long-term service, and these components may fracture due to repeated stress, which are much lower than the conventional static strength [32–35]. For example, Lara et al. [32] found that cutting technology affected the fatigue properties of Al-Si coated 22MnB5 high-strength steel sheets with ~1333 MPa of yield strength (YS) and ~1560 MPa of ultimate tensile strength (UTS). The endurance limits under 2×10^6 tension-tension loading cycles (load ratio $R = 0.1$) were 391 MPa and 453 MPa for sheared specimens and laser-cut specimens, respectively. With further grinding and polishing on the cutting edges of the sheared specimens, it dramatically increased up to 652 MPa. Considering that fatigue failure always bring catastrophic economic loss and casualties, it has received more interest in recent decades due to scientific as well as engineering requirements. However, investigations on the tension-compression fatigue behavior of hot-stamping high-strength boron steel sheet are limited. The main objective of this work was to characterize the phase evolution of Al-Si coating during hot stamping, and to reveal the effect of the high-cycle fatigue behavior on a commercial boron steel sheet. Our work indicated that the Al-Si coating could significantly improve the fatigue life.

2. Experimental Procedures

A comparison was made between two 1500 MPa-grade high-strength boron steel sheets, each 1.80 mm thick (B1500HS, Chinese grade, largely corresponds to 22MnB5). One sheet was uncoated and the other was coated with Al-Si by continuously using the hot-dipping method. Aside from the coating, both sheets had the same chemical composition (Table 1). Both types of cold-rolled steel sheets were heated to 1193 K at 30 K/s, held for 180 s, and then the austenized sheets were quickly cooled at ~70 K/s to the desired stamping temperature with the help of high pressure air. The stamping was done at a start temperature of ~973 K with a pressure time of 5 s in the present work. The YS and UTS of both sheets were ~1250 MPa and ~1500 MPa, respectively. High-cycle fatigue tests were conducted using a servo hydraulic tabletop test system (Bionix 370.02, MTS, Eden Prairie, MN, USA) with the load axis parallel to the rolling direction. The specimens for the fatigue test were wire-cut from the hot-stamped sheets, and the dimensions have been illustrated in Figure 1. More than five stress levels based on the standard staircase method were undertaken in stress control at room temperature. A sinusoidal waveform was employed at 20 Hz with fully reversed tension-compression loading (stress ratio $R = -1$). Care was taken to ensure the proper alignment of the specimen in the grips and to eliminate buckling of the specimen during fixing and testing. Three experiments were performed under each stress level, and if two of them reached 10^7 cycles, the endurance limit was considered to be reached.

Table 1. The chemical composition of the studied boron steel sheet (wt.%).

C	Si	Mn	P	S	Ni	Mo	Al	B	Cr	Ti	Cu
0.23	0.25	1.35	0.015	0.006	0.028	0.04	0.04	0.003	0.19	0.03	0.016

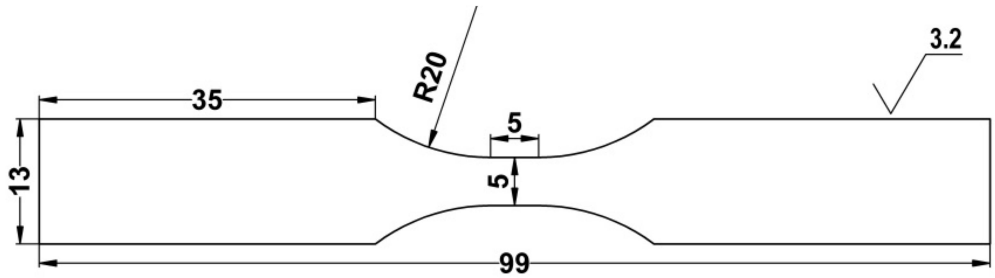

Figure 1. Illustration for dimensions of the fatigue test specimens (unit: mm).

The microstructure and fracture morphology were observed using stereomicroscope (SteREO Discovery V8, Zeiss International, Berlin, Germany) and an optical microscope (Zeiss A2m, Zeiss International, Berlin, Germany). Quantitative elemental analysis was conducted using a field emission electron probe microanalyzer (EPMA-8050G, Shimadzu, Tokyo, Japan). High-temperature differential scanning calorimetric measurements (DSC 404 F3, NETZSCH-Gerätebau GmbH, Selb, Germany) were carried out at a heating rate of 10 K/min. The martensitic transformation start temperature was determined on a dilatometer system (TA DIL805L, TA Instruments, Eschborn, Germany), and the experimental process was as follows: (1) heated to 1193 K at a heating rate of 1 K/s and kept for 180 s; (2) quenched to room temperature at a cooling rate of 20 K/s.

3. Results and Discussion

3.1. Al-Si Coating

The thickness of the Al-Si coating on the as-received boron steel sheet was approximately 30 μm on each side (Figure 2a). The steel substrate showed refined ferrite/pearlite [36]. A reaction between the substrate and the Al-Si coating (Layer I) produced a transition layer (Layer II). After hot stamping at 1193 K, the microstructure of Layer I indicated the formation of a new intermetallic compound with a few voids (Figure 2b). Layer II became thicker (~7 μm), and the steel substrate transformed into lath-like martensite.

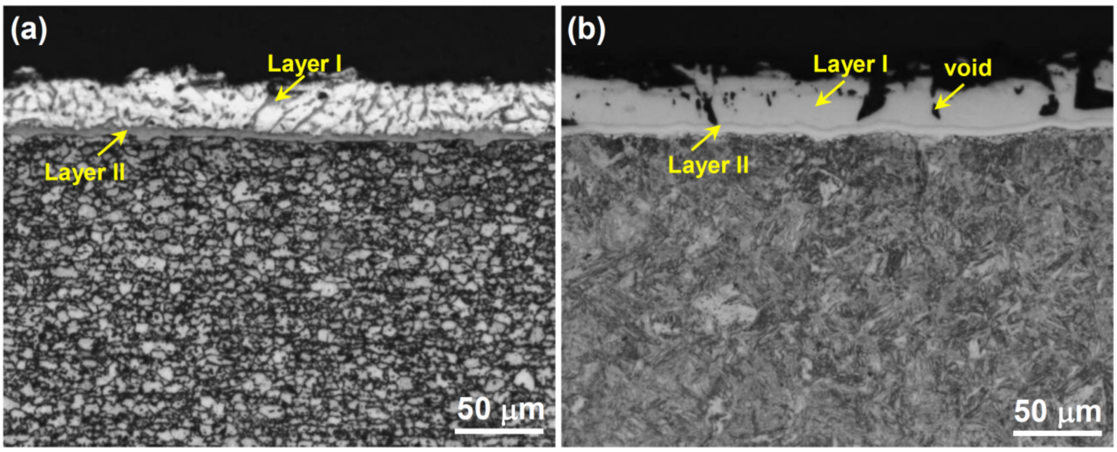

Figure 2. Cross-sectional optical microstructures of Al-Si coated specimens, as-received state (**a**) and after hot-stamped at 1193 K (**b**).

EPMA quantitative analyses showed that the dominant phases of Layer I in the as-received steel sheet were α(Al) matrix and eutectic Al-Si, while the dominant phase of Layer II was Fe_2Al_7Si (τ_5) ternary intermetallic compound (Figure 3a). After hot stamping at 1193 K, three new phases formed: Fe(Al,Si) (β_2), $Fe(Al,Si)_2$ and α(Fe) [17,28,37–39] (Figure 3b). It should be noticed that although these colors in Figure 3 are false colors assigned by the instrument program, they provide more differential contrast for human eye than the grey scale. The values corresponding to different color represent the number of photons detected by x-ray. The larger value indicates the higher content of the target element. The average chemical compositions of different phases at different locations have been listed in Table 2. All measurements were calibrated using pure elements, and five spots were performed for each phase. It is obvious that high-temperature hot stamping rapidly activated interdiffusion between the coating and the steel substrate, and because of the Kirkendall effect (that is, the movement between two metals that occurs with different diffusion rates), a few voids appeared inside the coating layer (Figures 2b and 3b) [17,28,40]. Cracks were also observed, which were closely linked to the differences between the thermal expansion coefficients of the newly-formed Fe-Al-Si phases in the coating [28].

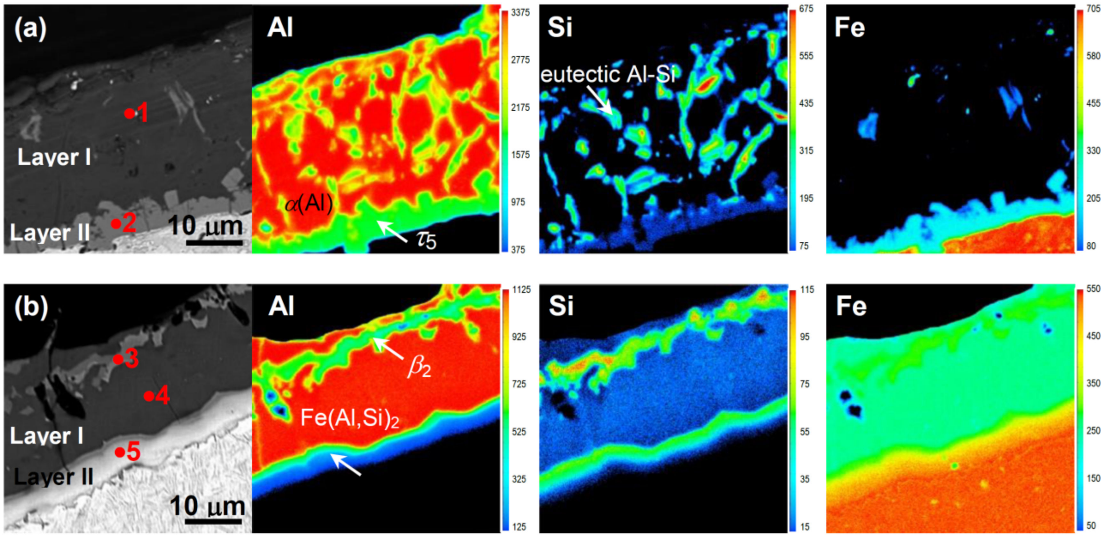

Figure 3. Backscattered electron images and the corresponding elemental distributions in Al-Si coated specimens, as-received state (**a**) and after hot-stamped at 1193 K (**b**). The average chemistry in location 1 of Figure 3a indicated the existence of α(Al) matrix and eutectic Al-Si phase. The average chemistry in location 2 of Figure 3a indicated that the dominant phase in Layer II was Fe_2Al_7Si (τ_5) ternary intermetallic compound. The average chemistries in locations 3, 4 and 5 in Figure 3b indicated formation of Fe(Al,Si) (β_2), $Fe(Al,Si)_2$ and α(Fe) phases, respectively.

Table 2. The average chemical compositions of different phases at locations 1–5 as marked in Figure 3 (at.%).

Element	1	2	3	4	5
Fe	0.2	21.0	51.3	33.5	85.0
Al	94.6	69.3	35.5	63.6	10.9
Si	5.2	9.7	13.2	2.9	4.1

The DSC chart showed three phase transitions of the coated steel sheet within the measured temperature range from 700 K and 1150 K (Figure 4a). The first endothermic peak at 845 K upon heating was attributed to the melting of eutectic Al-Si phase, and the second peak at 882 K indicated the melting of α(Al) phase according to the Al-Si binary phase diagram [41]. The third peak at 1014 K corresponded to the austenitization of boron steel [42], which was consistent with the dilatometric data (Figure 4b). A relative length contraction took place between 1010 K (Ac_1) and 1099 K (Ac_3) upon heating, corresponding to the start and finish of ferrite → austenite transformation, respectively [43]. The inflation started at 667 K upon cooling resulted from the martensitic transformation [44].

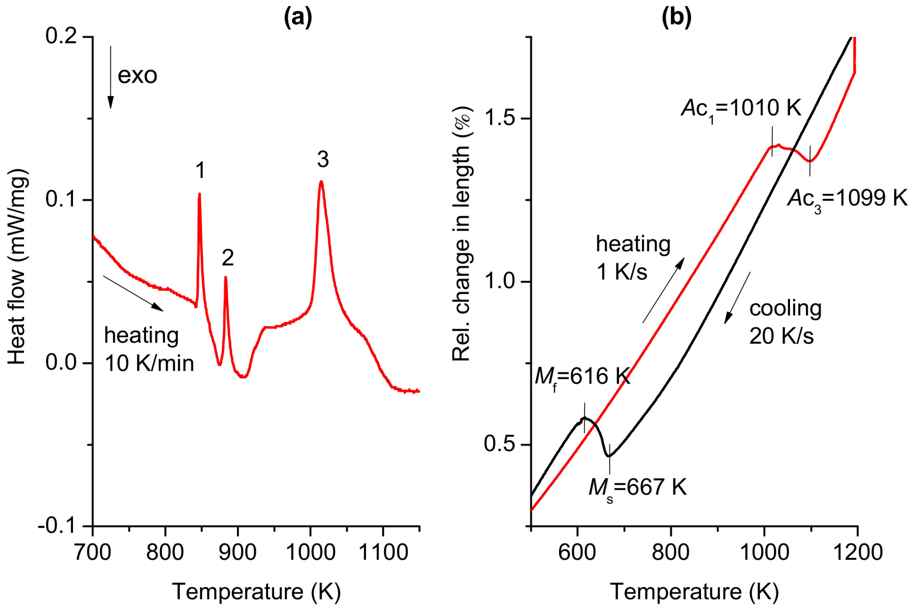

Figure 4. DSC (**a**) and dilatometric (**b**) curves of as-received Al-Si coated specimen.

The microstructures of steel substrate and the corresponding carbon (C) and aluminum (Al) elemental distributions were investigated in order to understand high-cycle fatigue behavior. In the hot-stamped coated specimen, lath-like martensite was observed (Figure 5a). Carbon distributed homogeneously in the substrate (Figure 5b). In the uncoated specimen, a decarburized layer with a width of approximately 80 µm was observed, where the carbon content was significantly lower relative to the interior region (Figure 5d). The number in the color bar of Figure 5 represents the area fraction of C/Al element within the measured area. It has been generally thought that decarburization is a surface degradation process involving the loss of near-surface carbon from steel during exposure in air at elevated temperatures, which would seriously deteriorate the mechanical properties of steels [45]. For example, Ren et al. [46] reported that the presence of decarburization reduced the microhardness from 425 HV to 260 HV in a 50CrMnMoVNb spring steel. Zhao et al. [47] found that the crack growth rate on the decarburized rail roller was over 4 times that of the non-decarburized rail roller under dry-wet conditions. Furthermore, the loss of the carbon element may have largely reduced the hardenability of the near-surface steel sheet [48] and thus the martensite transformation did not occur, and formed some ferrite/pearlite.

3.2. High-Cycle Fatigue Behavior

The statistic stress-fatigue life (*S-N*) curves obtained from two types of hot-stamped specimens showed that Al-Si coating enhanced fatigue endurance (Figure 6). At σ = 370 MPa stress level (stress amplitude), no Al-Si coated specimens failed at 10^7 cycles. Nonlinear logistic fit was used (OriginPro 8.5.0 SR1, Originlab Corporation, Northampton, MA, USA) and two equations, $\sigma = 391.326 + 112.691/\left[1 + \left(\frac{N}{100300.632}\right)^{5.329}\right]$ for Al-Si coated specimen and $\sigma = 305.305 + 299.709/\left[1 + \left(\frac{N}{79217.244}\right)^{0.995}\right]$ for the uncoated specimen, were obtained. At σ = 305 MPa, two uncoated specimens reached 10^7 cycles without failure. In other words, under 10^7 cycles of fully reverse tension-compression loading, the Al-Si coated steel sheet showed approximately 21% improvement of the endurance limit compared to the uncoated sheet. Low magnification images of fatigue fracture surface showed three distinctive fatigue regimes—crack initiation, propagation and final failure—for both coated and uncoated specimens (Figure 7a,c). Both types of specimens indicated surface-initiated failure, similar to the 22MnB5 steel sheets under a tension-tension loading mode [32]. The location of initiation, however, was different. Most of the cracks in the coated specimens were initiated on the side surface (which was created by using wire-cutting) (circled in Figure 7a). All fractures for the uncoated specimens generated inside the decarburization layer (Figure 7c). That is, the decarburization layer acted as weaker location compared to the wire-cutting surface in the uncoated specimens. Enlarged facture surface images showed typical transgranular fracture feature [49] in both types of specimens, as pointed by the arrows in Figure 7b,d.

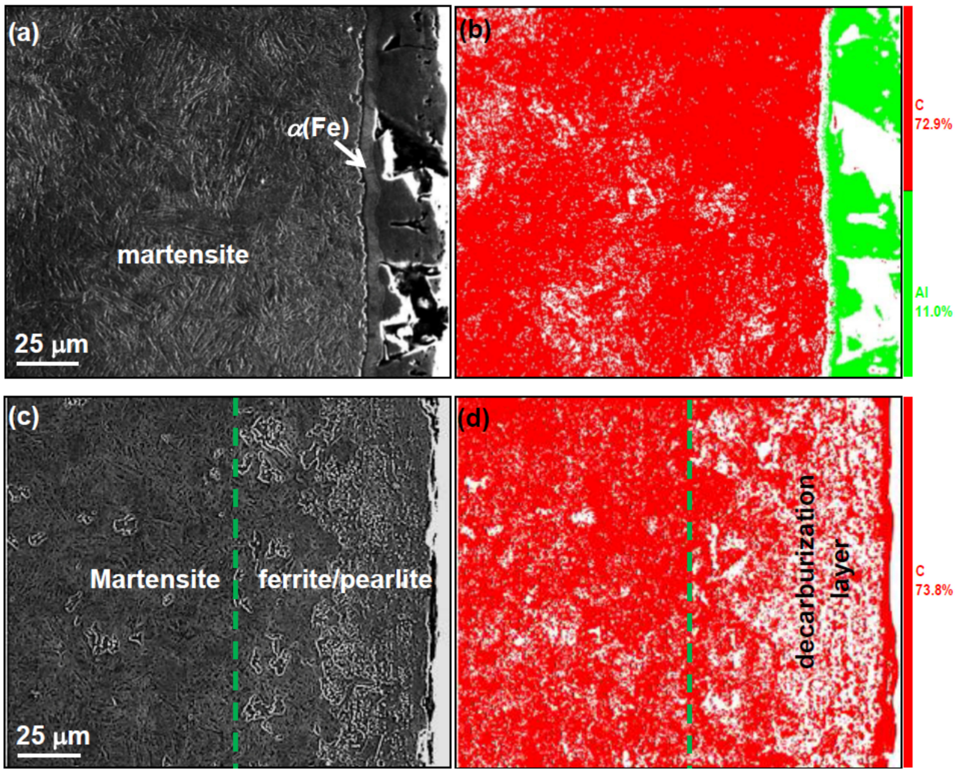

Figure 5. Cross-sectional SEM images and the corresponding C and Al elemental distributions after hot stamping at 1193 K for the coated (**a**,**b**) and uncoated (**c**,**d**) specimens.

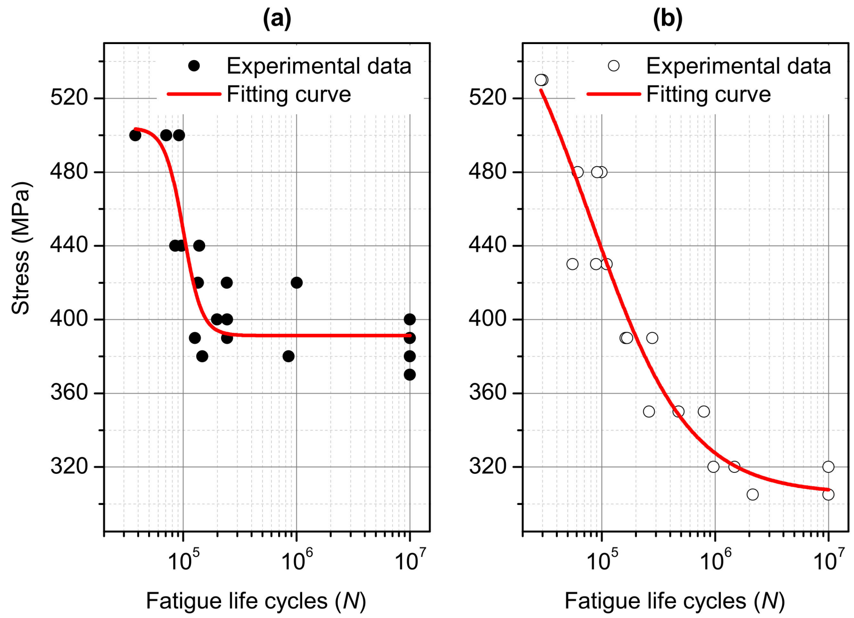

Figure 6. Stress-fatigue life (*S*-*N*) curves of Al-Si coated (**a**) and uncoated (**b**) specimens after hot stamping at 1193 K.

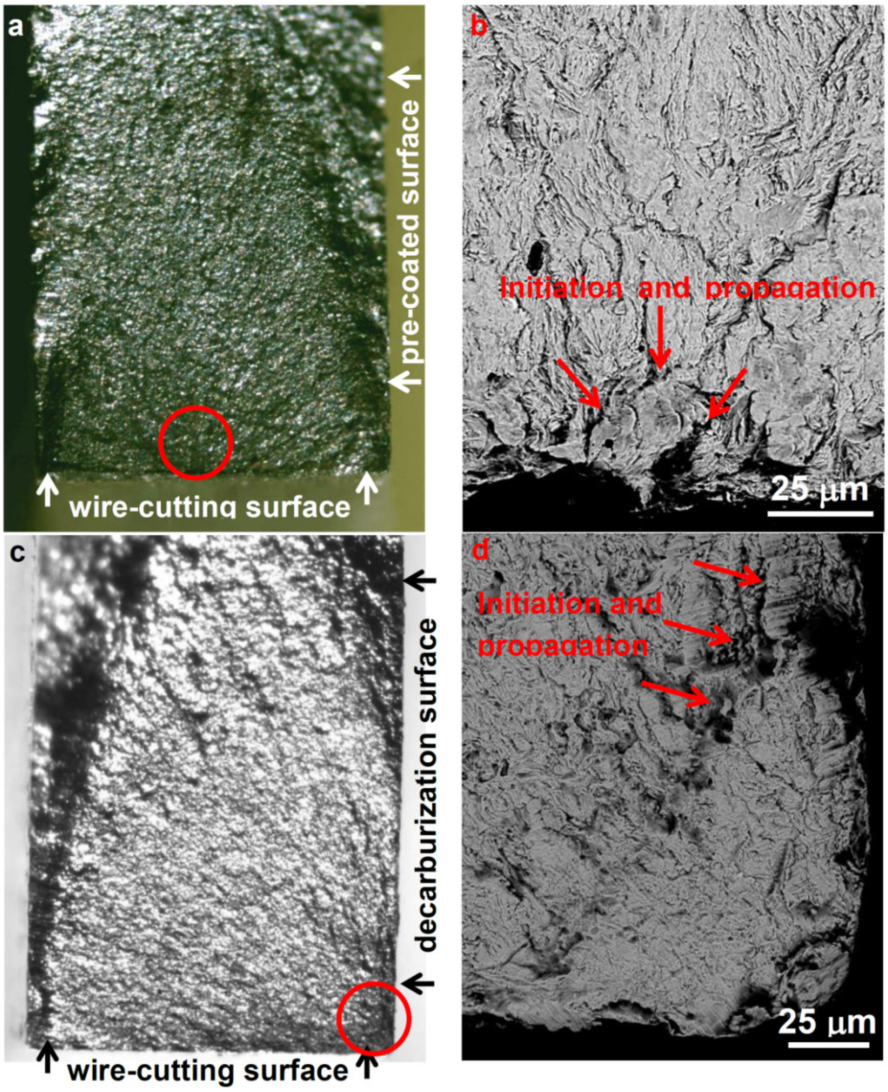

Figure 7. Fracture macrographs of coated (**a**) and uncoated (**c**) specimens under 390 MPa after hot stamping at 1193 K. (**b**,**d**) are the enlarged images showing the crack initiation and early propagation (marked by arrows).

The prediction of the crack initiation location was conducted to validate the microstructural observation. The numerical model was established (SOLIDWORKS®Premium 2016, SP 1.0, Dassault Systèmes, Waltham, MA, USA) and as described above, the decarburized layer on both sides of the uncoated specimen was preset with a thickness of 80 μm, and it was presumed that the UTS value linearly decreased from 1500 MPa to 900 MPa from the interface (green dashed line marked in Figure 5c) to the outer edge of the decarburization layer. The coated specimen was taken to be a uniform sheet for clarity since the narrow α(Fe) diffusion layer is less than 7 μm. Figure 8 demonstrates the cloud images of damage for the fatigue specimens obtained by the finite element method (ANSYS®Workbench^{TM} 2.0 Framework, 15.0.0, ANSYS, Inc., Canonsburg, PA, USA) under a sinusoidal tension-compression cyclic loading of 390 MPa. Miner's law was used based on the theory of linear cumulative damage. The fatigue damage was defined as the design life divided by the available life, and design life was preset at 10^9 in the present work. That is, the fatigue value is inversely proportional to the fatigue life cycles (N) and in the present work, it equaled $10^9/N$. The larger damage value indicated the shorter fatigue life where it was easier to initiate the crack. The weakest locations have been circled in Figure 8a,b, respectively. It can be seen that the simulation results agree well with the experimental observation of the wire-cutting surface for the coated specimen during cyclic loading. For the uncoated specimen, the fatigue cracks would be easier to generate inside the decarburization layer. According to this conclusion, it seems necessary to further address the effect of the cutting surface quality (integrity) for the application of Al-Si coated high-strength boron steel sheet as fatigue resistant components.

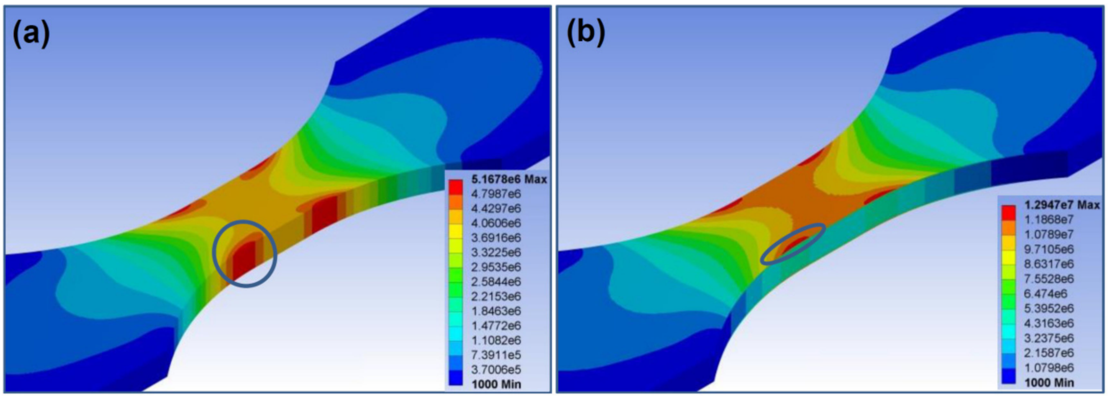

Figure 8. Cloud images of damage for the coated (**a**) and uncoated (**b**) fatigue specimens under 390 MPa obtained by the finite element method with a sinusoidal cyclic loading mode.

4. Conclusions

Two types of 1500 MPa grade hot stamping boron steel sheets were compared, one with Al-Si coating and the other without. The following conclusions were obtained.

(1) The phases of the as-received Al-Si coating were α(Al), eutectic Al-Si, and τ_5. After hot stamping at 1193 K, Fe(Al,Si)$_2$, β_2 and α(Fe), phases formed and some voids/cracks appeared inside the coating. The Al-Si coating effectively prevented the occurrence of near-surface decarburization during high-temperature hot stamping.

(2) The endurance limit of the hot-stamped coated steel sheet was 370 MPa compared to 305 MPa for the uncoated sheet under 10^7 fully reversed tension-compression loading cycles. Both specimens were classified as the surface-induced transgranular fatigue fracture.

(3) The high-cycle fatigue cracks were generated from the decarburization layer in the uncoated sheet, whereas for the coated sheet, the cracks were initiated at wire-cutting surfaces.

Author Contributions: Formal analysis, Y.L., N.T., Z.X., Z.L. and K.H.; investigation, Y.L. and H.Z.; methodology, H.Z.; supervision, H.Z.; writing – original draft, Y.L.; writing–review & editing, N.T., Z.L., K.H. and Q.Z.

Funding: This research was funded by the National Key Research and Development Program of China (2018YFB0704403) and the Shanghai Sailing Program (17YF1405900).

Acknowledgments: The authors are grateful to the National Key Research and Development Program of China and the Shanghai Sailing Program, which enabled the research to be carried out successfully. We thank Tyler for preliminary editing of the manuscript.

Conflicts of Interest: The authors declare no conflicts of interest.

References

1. Merklein, M.; Wieland, M.; Lechner, M.; Bruschi, S.; Ghiotti, A. Hot stamping of boron steel sheets with tailored properties: A review. *J. Mater. Process. Tech.* **2016**, *228*, 11–24. [CrossRef]
2. Li, N.; Lin, J.; Balint, D.S.; Dean, T.A. Modelling of austenite formation during heating in boron steel hot stamping processes. *J. Mater. Process. Tech.* **2016**, *237*, 394–401. [CrossRef]
3. Mori, K.; Bariani, P.F.; Behrens, B.-A.; Brosius, A.; Bruschi, S.; Maeno, T.; Merklein, M.; Yanagimoto, J. Hot stamping of ultra-high strength steel parts. *CIRP Ann.* **2017**, *66*, 755–777. [CrossRef]
4. Abdulhay, B.; Bourouga, B.; Dessain, C. Experimental and theoretical study of thermal aspects of the hot stamping process. *Appl. Therm. Eng.* **2011**, *31*, 674–685. [CrossRef]

5. Shao, Z.; Lin, J.; Ganapathy, M.; Dean, T. Experimental and modelling techniques for hot stamping applications. *Procedia Manuf.* **2018**, *15*, 6–13. [CrossRef]
6. Nakagawa, Y.; Mori, K.; Yashima, S.; Kaido, T. Springback behaviour and quenchability in hot stamping of thick sheets. *Procedia Manuf.* **2018**, *15*, 1071–1078. [CrossRef]
7. George, R.; Bardelcik, A.; Worswick, M.J. Hot forming of boron steels using heated and cooled tooling for tailored properties. *J. Mater. Process. Tech.* **2012**, *212*, 2386–2399. [CrossRef]
8. Bariani, P.F.; Bruschi, S.; Ghiotti, A.; Turetta, A. Testing formability in the hot stamping of HSS. *CIRP Ann.* **2008**, *57*, 265–268. [CrossRef]
9. Karbasian, H.; Tekkaya, A.E. A review on hot stamping. *J. Mater. Process. Tech.* **2010**, *210*, 2103–2118. [CrossRef]
10. Neumann, R.; Schuster, S.; Gibmeier, J.; Böhlke, T. Two-scale simulation of the hot stamping process based on a Hashin-Shtrikman type mean field model. *J. Mater. Process. Tech.* **2019**, *267*, 124–140. [CrossRef]
11. Lu, Y.; Peer, A.; Abke, T.; Kimchi, M.; Zhang, W. Subcritical heat affected zone softening in hot-stamped boron steel during resistance spot welding. *Mater. Design* **2018**, *155*, 170–184. [CrossRef]
12. Li, X.D.; Chang, Y.; Wang, C.Y.; Hu, P.; Dong, H. Comparison of the hot-stamped boron-alloyed steel and the warm-stamped medium-Mn steel on microstructure and mechanical properties. *Mater. Sci. Eng. A* **2017**, *679*, 240–248. [CrossRef]
13. Xing, Z.W.; Bao, J.; Yang, Y.Y. Numerical simulation of hot stamping of quenchable boron steel. *Mater. Sci. Eng. A* **2019**, *499*, 28–31. [CrossRef]
14. Fan, D.W.; Kim, H.S.; De Cooman, B.C. A review of the physical metallurgy related to the hot press forming of advanced high strength steel. *Steel Res. Int.* **2009**, *80*, 241–248. [CrossRef]
15. Mori, K.; Ito, D. Prevention of oxidation in hot stamping of quenchable steel sheet by oxidation preventive oil. *CIRP Ann.* **2009**, *58*, 267–270. [CrossRef]
16. Allély, C.; Dosdat, L.; Clauzeau, O.; Ogle, K.; Volovitch, P. Anticorrosion mechanisms of aluminized steel for hot stamping. *Surf. Coat. Tech.* **2014**, *238*, 188–196. [CrossRef]
17. Fan, D.W.; De Cooman, B.C. State-of-the-knowledge on coating systems for hot stamped parts. *Steel Res. Int.* **2012**, *83*, 412–433. [CrossRef]
18. Zhang, J.; Jiang, S.; Zhang, Q.; Liu, C. Effect of temperature on microstructure and formability of Al-10 mass% Si coatings. *J. Iron. Steel Res. Int.* **2016**, *23*, 270–275. [CrossRef]
19. Pelcastre, L.; Hardell, J.; Rolland, A.; Prakash, B. Influence of microstructural evolution of Al-Si coated UHSS on its tribological behaviour against tool steel at elevated temperatures. *J. Mater. Process. Tech.* **2016**, *228*, 117–124. [CrossRef]
20. Windmann, M.; Röttger, A.; Theisen, W. Phase formation at the interface between a boron alloyed steel substrate and an Al-rich coating. *Surf. Coat. Tech.* **2013**, *226*, 130–139. [CrossRef]
21. Dosdat, L.; Petitjean, J.; Vietoris, T.; Clauzeau, O. Corrosion resistance of different metallic coatings on press-hardened steels for automotive. *Steel Res. Int.* **2011**, *82*, 726–733. [CrossRef]
22. Ighodaro, O.L.; Biro, E.; Zhou, Y.N. Comparative effects of Al-Si and galvannealed coatings on the properties of resistance spot welded hot stamping steel joints. *J. Mater. Process. Tech.* **2016**, *236*, 64–72. [CrossRef]
23. Chang, J.K.; Lin, C.S.; Wang, W.R.; Cheng, W.J. Microstructural evaluation and property change of 5 wt pct Al-Zn coating on press hardening steel during austenitization. *Metall. Mater. Trans. A* **2018**, *49*, 3715–3728. [CrossRef]
24. Kondratiuk, J.; Kuhn, P.; Labrenz, E.; Bischoff, C. Zinc coatings for hot sheet metal forming: Comparison of phase evolution and microstructure during heat treatment. *Surf. Coat. Tech.* **2011**, *205*, 4141–4153. [CrossRef]
25. Kondratiuk, J.; Kuhn, P. Tribological investigation on friction and wear behaviour of coatings for hot sheet metal forming. *Wear* **2011**, *270*, 839–849. [CrossRef]
26. Alibakhshi, E.; Akbarian, M.; Ramezanzadeh, M.; Ramezanzadeh, B.; Mahdavian, M. Evaluation of the corrosion protection performance of mild steel coated with hybrid sol-gel silane coating in 3.5 wt.% NaCl solution. *Prog. Org. Coat.* **2018**, *123*, 190–200. [CrossRef]
27. Lee, C.W.; Choi, W.S.; Cho, Y.R.; De Cooman, B.C. Microstructure evolution of a 55 wt.% Al-Zn coating on press hardening steel during rapid heating. *Surf. Coat. Tech.* **2005**, *281*, 35–43. [CrossRef]
28. Gui, Z.X.; Wang, K.; Zhang, Y.S.; Zhu, B. Cracking and interfacial debonding of the Al-Si coating in hot stamping of pre-coated boron steel. *Appl. Surf. Sci.* **2014**, *316*, 595–603. [CrossRef]

29. Yao, S.J.; Feng, L.; Yang, D.L.; Han, D.X.; Liu, Y.; Li, Q.Q.; Guo, J.H.; Chao, B.J. A potential hot stamping process for microstructure optimization of 22MnB5 steels characterized by asymmetric pre-rolling and one- or two-step pre-heating. *J. Mater. Process. Tech.* **2018**, *254*, 100–107. [CrossRef]
30. Golling, S.; Frómeta, D.; Casellas, D.; Jonsén, P. Influence of microstructure on the fracture toughness of hot stamped boron steel. *Mater. Sci. Eng. A* **2019**, *743*, 529–539. [CrossRef]
31. Ganapathy, M.; Li, N.; Lin, J.; Bhattacharjee, D. Investigation of a new hot stamping process with improved formability and productivity. *Procedia Eng.* **2017**, *207*, 771–776. [CrossRef]
32. Lara, A.; Picas, I.; Casellas, D. Effect of the cutting process on the fatigue behaviour of press hardened and high strength dual phase steels. *J. Mater. Process. Tech.* **2013**, *213*, 1908–1919. [CrossRef]
33. Majumdar, S.; Bhattacharjee, D.; Ray, K.K. Mechanism of fatigue failure in interstitial-free and interstitial-free high-strength steel sheets. *Scripta Mater.* **2011**, *64*, 288–291. [CrossRef]
34. Zhao, P.; Cheng, C.; Gao, G.; Hui, W.; Misra, R.D.K.; Bai, B.; Weng, Y. The potential significance of microalloying with niobium in governing very high cycle fatigue behavior of bainite/martensite multiphase steels. *Mater. Sci. Eng. A* **2016**, *650*, 438–444. [CrossRef]
35. Park, S.H.; Lee, C.S. Relationship between mechanical properties and high-cycle fatigue strength of medium-carbon steels. *Mater. Sci. Eng. A* **2017**, *690*, 185–194. [CrossRef]
36. Hou, H.; Li, H.; He, L.; Tang, B. Analysis of phase transformation and blanking accuracy of B1500HS steel during hot blanking. *Procedia Eng.* **2017**, *207*, 1528–1533. [CrossRef]
37. Sun, Y.M.; Wu, L.J.; Tan, C.W.; Zhou, W.L.; Chen, B.; Song, X.G.; Zhao, H.Y.; Feng, J.C. Influence of Al-Si coating on microstructure and mechanical properties of fiber laser welded 22MnB5 steel. *Opt. Laser Technol.* **2019**, *116*, 117–127. [CrossRef]
38. Fan, D.W.; Kim, H.S.; Oh, J.K.; Chin, K.G.; Cooman, B.C. Coating degradation in hot press forming. *ISIJ Int.* **2010**, *50*, 561–568. [CrossRef]
39. Maitra, T.; Gupta, S.P. Intermetallic compound formation in Fe–Al–Si ternary system: Part II. *Mater. Charact.* **2003**, *49*, 293–311. [CrossRef]
40. Tavoosi, M. The Kirkendall void formation in Al/Ti interface during solid-state reactive diffusion between Al and Ti. *Surf. Interfaces* **2017**, *9*, 196–200. [CrossRef]
41. Haque, A.; Shekhar, S.; Narayana Murty, S.V.S.; Ramkumar, J.; Kar, K.; Mondal, K. Fabrication of controlled expansion Al-Si composites by pressureless and spark plasma sintering. *Adv. Powder Technol.* **2018**, *29*, 3427–3439. [CrossRef]
42. Grauer, S.J.; Caron, E.J.F.R.; Chester, N.L.; Wells, M.A.; Daun, K.J. Investigation of melting in the Al-Si coating of a boron steel sheet by differential scanning calorimetry. *J. Mater. Process. Tech.* **2015**, *216*, 89–94. [CrossRef]
43. Deirmina, F.; Peghini, N.; AlMangour, B.; Grzesiak, D.; Pellizzari, M. Heat treatment and properties of a hot work tool steel fabricated by additive manufacturing. *Mater. Sci. Eng. A* **2019**, *753*, 109–121. [CrossRef]
44. Namklang, P.; Uthaisangsuk, V. Description of microstructures and mechanical properties of boron alloy steel in hot stamping process. *J. Manuf. Process.* **2016**, *21*, 87–100. [CrossRef]
45. Mercier, D.; Lesage, J.; Decoopman, X.; Chicot, D. Eddy currents and hardness testing for evaluation of steel decarburizing. *NdT&E Int.* **2006**, *39*, 652–660. [CrossRef]
46. Ren, C.X.; Wang, D.Q.; Wang, Q.; Guo, Y.S.; Zhang, Z.J.; Shao, C.W.; Yang, H.J.; Zhang, Z.F. Enhanced bending fatigue resistance of a 50CrMnMoVNb spring steel with decarburized layer by surface spinning strengthening. *Int. J. Fatigue* **2019**, *124*, 277–287. [CrossRef]
47. Zhao, X.J.; Wang, H.Y.; Guo, J.; Liu, Q.Y.; Zhao, G.T.; Wang, W.J. The effect of decarburized layer on rolling contact fatigue of rail materials under dry-wet conditions. *Eng. Fail. Anal.* **2018**, *91*, 58–71. [CrossRef]
48. Van Hall, S.N.; Findley, K.O.; Freis, A.K. Improved self-pierce rivet performance through intentional decarburization. *J. Mater. Process. Tech.* **2018**, *251*, 350–359. [CrossRef]
49. Fan, Y.; Zhao, X.; Liu, Y. Research on fatigue behavior of the flash welded joint enhanced by ultrasonic peening treatment. *Mater. Design* **2016**, *94*, 515–522. [CrossRef]